HHS Public Access

Author manuscript

Nat Microbiol. Author manuscript; available in PMC 2019 February 27.

Published in final edited form as:

Nat Microbiol. 2018 October ; 3(10): 1090–1098. doi:10.1038/s41564-018-0222-7.

EXP2 is a nutrient-permeable channel in the vacuolar membrane of *Plasmodium* and is essential for protein export via PTEX

Matthias Garten[1], **Armiyaw S. Nasamu**[2], **Jacquin C. Niles**[3], **Joshua Zimmerberg**[1], **Daniel E. Goldberg**[2], and **Josh R. Beck**[2,4]

[1]Section on Integrative Biophysics, Eunice Kennedy Shriver National Institute of Child Health and Human Development, National Institutes of Health, Bethesda, MD, 20892, USA

[2]Departments of Medicine and Molecular Microbiology, Washington University School of Medicine, St. Louis, MO 63110, USA

[3]Department of Biological Engineering, Massachusetts Institute of Technology, Cambridge, MA 02139, USA

[4]Department of Biomedical Sciences, Iowa State University, Ames, IA 50011 USA.

Intraerythrocytic malaria parasites reside within a parasitophorous vacuolar membrane (PVM) generated during host cell invasion[1]. Erythrocyte remodeling and parasite metabolism respectively require export of effector proteins and transport of small molecules across this barrier between the parasite surface and host cell cytosol[2,3]. Protein export across the PVM is accomplished by the *Plasmodium* translocon of exported proteins (PTEX) consisting of three core proteins including the AAA+ ATPase HSP101 and two additional proteins known as PTEX150 and EXP2[4]. Inactivation of HSP101 and PTEX150 arrests protein export across the PVM[5,6], but the contribution of EXP2 to parasite biology is not well understood[7]. At the same time, a nutrient permeable channel in the PVM has been characterized electrophysiologically, but its molecular identity is unknown[8,9]. Here, using regulated gene expression, mutagenesis and cell-attached patch clamp measurements, we show that EXP2, the putative membrane-spanning channel of PTEX[4,10–14], serves dual roles as a protein-conducting channel in the context of PTEX and as a channel able to facilitate nutrient passage across the PVM independent of HSP101. Our data suggest a dual functionality for a channel operating in its endogenous context.

To interrogate EXP2 function in the intraerythrocytic cycle of *Plasmodium falciparum*, we employed the recently developed TetR-DOZI-aptamer system[15,16] to achieve conditional control of EXP2 translation in a clonal parasite line designated EXP2^{apt} (Fig. 1a and

Correspondence to: Joshua Zimmerberg; Daniel E. Goldberg.

Author Contributions

M.G., J.Z., D.E.G. and J.R.B. conceived and designed experiments. M.G. and J.R.B. performed the experiments. J.R.B. generated and analyzed the parasite strains. M.G. performed patch clamp analysis. A.S.N. generated the pEXP2^{apt} plasmid. J.C.N. contributed reagents. M.G., J.Z., D.E.G. and J.R.B. analyzed the data and wrote the manuscript. All authors discussed and edited the manuscript.

Author Information

Reprints and permissions information is available at www.nature.com/reprints. The authors declare no competing financial interests. Correspondence and requests for materials should be addressed to D.E.G. (dgoldberg@wustl.edu) and J.Z. (zimmerbj@mail.nih.gov).

Supplementary Fig. 1). In the presence of anhydrotetracycline (aTc), EXP2^{apt} parasites showed a ~60% reduction in basal EXP2 expression by western blot and displayed a growth defect relative to the parental line (Fig. 1b, c). Removal of aTc from the culture resulted in further reduction of EXP2 levels to less than 10% of the parent in 48 h and a complete block in replication, demonstrating an essential requirement of EXP2 for blood-stage survival. We also observed a correlation between the number of merozoites produced per infected red blood cell (RBC) and EXP2 expression levels (Supplementary Fig. 2), demonstrating EXP2 is important for fitness in the later stages of the parasite developmental cycle[17].

Similar to other PTEX core components[5,6], depletion of EXP2 resulted in a severe defect in export of effector proteins beyond the PVM (Fig. 1d, e). This was accompanied by abnormalities in PV morphology which could be visualized in Giemsa-stained thin smears (Supplementary Fig. 3) and revealed by transmission electron microscopy to be tubular distensions of the PVM projecting into the erythrocyte cytosol, in contrast to the normal tight apposition of the PVM to the parasite plasma membrane (PPM) (Fig. 1f). To test the impact on PV morphology of inactivating a distinct PTEX core component, we utilized a previously reported approach for post-translational conditional inactivation of HSP101[5] which we regenerated in the NF54^{attB} background used in the present study (Supplementary Fig. 4). In this system, a mutant, unstructured version of *E. coli* DHFR is fused to the endogenous C-terminus of HSP101. Normal function is maintained in the presence of trimethoprim (TMP) while withdrawal of this stabilizing ligand leads to rapid inactivation of HSP101. Similar PVM distensions were observed following conditional inactivation of HSP101 (Fig. 1g) and presumably arise from buildup of blocked exported proteins in the PV lumen that either directly expand the volume of the PV or alter the osmotic balance within the compartment, leading to swelling. Specificity of exported protein trafficking through PTEX has been hypothesized to occur either through recognition of unique export signals on cargo secreted into the PV lumen, or through dedicated export subcompartments to which PTEX has privileged access[18]. That PVM distension arise from discrete points rather than presenting as a uniform PVM swelling is better explained by the later model. We tested this possibility with a split GFP approach modeled after a previously reported sub-compartmental split GFP strategy in *P. falciparum*[19]. This system enabled us to monitor the PTEX accessibility of a soluble GFP1–10 reporter targeted to the PV lumen. Vacuolar GFP fluorescence was observed when a GFP11 tag was fused to the endogenous C-terminus of EXP2, PTEX150 or HSP101, indicating that PTEX components are freely accessible by diffusion of non-exported proteins in the PV lumen (Supplementary Fig. 5). This argues against export-dedicated subcompartments and suggests that other constraints, such as possible sites of PVM-PPM anchoring, contribute to the formation of the distensions observed upon EXP2 or HSP101 knockdown. These split GFP assays also indicate that the C-terminus of EXP2 resides within the PV lumen.

Peak expression of HSP101 and PTEX150 begins in late schizogony during merozoite formation and extends into the early ring stage shortly after invasion[11,20], overlapping with the expression of many exported proteins early in intraerythrocytic development during a period of dramatic host cell remodeling[21]. In contrast, EXP2 transcription peaks later[20], achieving higher transcript abundance than HSP101 and PTEX150 (Fig. 2a). Pulse-chase experiments indicated EXP2 synthesis also peaks later[11] and time-resolved western blots of

tightly synchronized parasites revealed increasing ratios of EXP2 relative to HSP101 as development proceeds (Fig. 2b). Furthermore, the majority of EXP2 was not co-purified with depleting immunoprecipitation of HSP101, particularly in the later part of the cycle when EXP2 levels are highest (Fig. 2c). These results suggest EXP2 may serve additional roles beyond PTEX-mediated protein export.

Disruption of EXP2 orthologs in the related apicomplexan *Toxoplasma gondii* results in a defect in small molecule transport (but not protein export) across the PVM that can be rescued by complementation with *P. falciparum* EXP2[13]. The *Toxoplasma* PVM channel[22] is thought to have similar characteristics to a nutrient-permeable PVM channel of unknown molecular identity in *P. falciparum*, which was characterized by on-cell patch clamp and is thought to play a crucial role in nutrient acquisition[8,9]. As EXP2 is thought to form the protein-conducting PVM channel in PTEX, we tested the hypothesis that EXP2 is also the PVM nutrient-permeable channel[3,13,23]. We found that after iso-osmotic bulk release from the host RBCs, parasites remained within their PVM available for patch clamp recording of membrane permeability, detected as ionic current[24] (Fig. 3a, b). Application of voltage revealed a channel permeable to nutrient-sized ions such as N-Methyl-D-glucamine and glutamate (Fig. 3c). Conductance of the patched PVM was typically in the nanosiemens range and showed step-wise currents when ~ +30 or ~ −60 mV were applied to the pipette electrode (Fig. 3d, e). Observed step sizes were variable (mode ~190 pS); largest steps were ~230 pS (Supplementary Fig. 6), consistent with sub-conductance states described previously for the PVM when scaling conductance for ion concentration[8]. A full channel conductance (~300 pS) can be estimated from step-wise decrements in conductance (presumably channels diffusing out of the patch, Supplementary Fig. 7), comparable to previous reports[9]. The reversal potential, close to 0 mV, was estimated from the current response to a step of voltage (Fig. 3f). From these steps, a conductance-voltage (G-V) response was constructed for each patch (Fig. 3g). The G-V response was maximal near zero transmembrane potential and diminished with both positive and negative voltages ($V_{half\text{-}open,\ positive}$ = 29±2 mV and $V_{half\text{-}open,\ negative}$ = −63±2 mV), also consistent with previous reports[9,25]. No other discernable channels were observed here, i.e. in absence of the channel activity noted above, patches had a resistance of several gigaohms. Channel rundown and the lipid-glass interactions inherent to patch clamping[26] prevented an estimate of channel densities; attempts at total channel count by accessing a “whole-vacuole” configuration were unsuccessful. Instead, relative PVM channel density was derived as the ‘frequency of channel detection’ (f_{chan}): the probability of observing at least one PVM channel in a given patch as determined from a series of patches.

If EXP2 constitutes the PVM channel, then f_{chan} should depend upon EXP2 expression. We compared parasites expressing a second copy of EXP2 (~150% wild-type EXP2 levels by western blot, Supplementary Fig. 2), the parental strain (100%), $EXP2^{apt}$ +aTc (~40%) and $EXP2^{apt}$ -aTc (~10%). There was a tight correlation between f_{chan} and expression of EXP2 (Fig. 3h, R=0.98). In contrast, conditional inactivation of HSP101 did not change f_{chan} (Fig. 3i), nor the PVM channel sub-conductance states and voltage response (Supplementary Fig. 8), suggesting that EXP2 function in the PVM channel is independent of its role in the PTEX complex.

If EXP2 is a component of the PVM channel, changes to the EXP2 sequence should alter the electrophysiological characteristics of the channel. The C-terminal 54 residues of EXP2 (S234-E287) are highly charged (Supplementary Fig. 9, 28 negatively charged residues and 6 positively charged residues) and are poorly conserved among apicomplexans outside the *Plasmodium* genus, suggesting that alternation of this region of EXP2 may not altogether compromise function[13]. Indeed, complementation of EXP2^{apt} with full length EXP2 or a truncated version lacking residues 234–287 both rescued growth and export following aTc washout (Supplementary Fig. 9). The charged truncated region comprising residues 234–287 is predicted to be in the aqueous space outside the lipid bilayer (Supplementary Fig. 5). Rather than sensing the trans-membrane potential, those charges can be expected to sense the potential gradient created by the access resistance of the channel[27,28] (Fig. 4a). Indeed, following aTc washout to deplete endogenous EXP2, EXP2^{apt}::Δ234–287 parasites displayed a PVM channel with altered voltage response. The half-open state with positive and negative voltages was substantially shifted away from 0 mV compared to the parent line, consistent with a diminished voltage response (Fig. 4 b-d). Single step conductance was not changed (Supplementary Fig. 10). When expression of full-length EXP2 was induced by the presence of aTc, a heterogeneous voltage response was recorded, consistent with mixed oligomers of full length and truncated EXP2 forming the PVM channel (Supplementary Fig. 10). The slope value of the voltage response was altered significantly for positive applied voltages (Fig. 4 e, f), consistent with a reduction in apparent gating charge (Fig. 4 g, h), in accordance with the concept of charge coupling in the region of pore access resistance.

The altered voltage response of the truncation mutant directly indicates EXP2 gates the PVM channel. Together with the dependence of f_{chan} on EXP2 expression and the observation that EXP2 forms a heptameric PVM pore in the context of PTEX[29], the most likely explanation of the data is that EXP2 is the nutrient-permeable PVM channel. Taken together, our results indicate critical functions of EXP2 as the PTEX protein-translocating pore and the nutrient-permeable channel of the PVM. There is no precedent for a channel protein performing such dual functions. While other PTEX components are unique to *Plasmodium* spp.[4], EXP2 is conserved amongst vacuole-dwelling apicomplexans[13] and appears to have been further adapted to function as a protein conducting channel by PTEX150/HSP101 in blood-stage malaria parasites. It remains to be seen if the nutrient-permeable PVM channel is formed in the context of PTEX, by EXP2 alone or by EXP2 with non-PTEX co-factors. Of these possibilities, the latter two seem to fit with the observations of the expression mismatch between EXP2 and the other PTEX components and the independence of the PVM channel from HSP101 function.

Methods

Parasite culture

For electrophysiology and IMF experiments parasites were cultured in human red blood cells obtained from donors participating in the NIH IRB-approved Research Donor Program in Bethesda, MD. Red blood cells were separated from other blood cells and serum by spinning it down 4x in RPMI 1640. Parasites were cultured in 5% hematocrit at 1–5% parasitemia in RPMI 1640 medium supplemented with with 25 mM HEPES, 0.1 mM

hypoxanthine, 25 μg/ml gentamicin, 0.5% Albumax II (all from Gibco, Waltham, MA), and 4.5 mg/ml glucose (Sigma, St. Louis, MO). For all other experiments, de-identified, IRB-exempt expired RBCs were obtained from the blood bank at the St. Louis Children's Hospital or directly from the American Red Cross and parasite culture was performed as described with the exception that RPMI was supplemented with 0.5% Albumax I[30]. Mutant lines were kept under selection drug pressure while cultured.

Genetic modification of *P. falciparum*

Cloning was carried out by Infusion (Clontech) unless otherwise noted. For editing the *exp2* genomic locus, the pre-single guide RNA (sgRNA) expression cassette was cut from the plasmid pAIO[31] by digestion with *NotI* and ligated into the *NotI* site in the plasmid pUF-1[32]. The Cas9–2xNLS-FLAG coding sequence was then amplified from pAIO with primers CCACATTTCGAATAAACTCGAGATGGACAAGAAGTACAGCATCGGCC and GACCTGCAGGGTACCCCCGGGTTACTTGTCGTCGTCGTCCTTGTAGTCCACTTTCCGCTTTTTCTTAG G and inserted between *XhoI* and *XmaI* in the pUF-1-pre-sgRNA plasmid, replacing the *yFCU* marker and placing Cas9 under control of the *hsp86* promoter and *PbDT* 3' UTR, resulting in the plasmid pUF-Cas9-pre-sgRNA. A Cas9 target was chosen downstream of the *exp2* stop codon (ATATTATGTACAGTATCTGA) and the guide RNA seed sequence was synthesized as a sense and anti-sense primer pair (sense shown) TAAGTATATAATATTATATTATGTACAGTATCTGAGTTTTAGAGCTAGAA. The primers were annealed and inserted into the *BtgZI* site of pUF-Cas9-pre-sgRNA to yield the plasmid pUF-Cas9-EXP2-CT-gRNA. For installation of aptamers at the *exp2* locus, a 5' homology flank was amplified with primers TTCAAACTTCATTGACTGTGCCCAAGTTGAGAACAAAAAATATTCTATACATGTTACTTC and GAGCTCCGGCAAATGACAAGGGCCGGCCCAAACTACAGTGTTTGTATTTTTATATACGAAGAATAACA AAAAAAAGGAAAATATATAACTGACTTTAATTTTAAAA from NF54^{attB} genomic DNA and by inserted by Gibson assembly (NEB) into a pJAZZ-based plasmid carrying the necessary TetR-DOZI-aptamer components[16] at *FseI*. A 3' flank beginning just downstream of the gRNA target site was amplified with primers TACGGTACAAACCCGGAATTCGAGCTCGGGTACAGTATCTGATGGAGAAACAATCTTTTA and ATTGGGTATTAGACCTAGGGATAACAGGGTAATTCATAAGGAGAGTACATAAATAAAATAATCAAAC and inserted at *I-SceI* with Gibson assembly. The *exp2* coding sequence (without introns) was recoded to a *Saccharomyces cerevisiae* codon bias and synthesized as a gene block (IDT) with a 3xHA tag (lower case indicates Gibson assembly overhangs):

ggtgatgttgaagaaaatccaggtccaATGAAAGTAAGCTATATCTTTTCCTTTTTTCTGTTGTTCTT
TGTCTATAAGAATACAAACACGGTTGTGTGTGATAACGGTTATGGGGATTTAGCGGCAACTTCAGCCT
TAACTACCGTCATAAAGGACCCAATCTCCTTGACGATAAAAGACATCTATGAACACGGTGTCAAAAAT
CCTTTTACTAAAATCATTCATAAGTTGAAGAAATTTATCAGGTATAGAAAAGTATTAAGATGGTCTAG
AATGTGGTGGGTATTGCTTGTTCGTGAGATTGTTGGAGATAATACGATTGAAAAGAAGACAGAGAAGG
CATTAAGAGAAATTTGGGACCAATGCACAATTGCCGTTTACAATAATACCCTTAATGCTGTAGAATCC
AAACCATTATTGTTCCTGCATGGTATACTAAATGAATGTAGAAATAATTTCGCCACAAAACTACGTCA
AGACCCTTCTCTAATTGTGGCAAAGATCGACCAAATCATAAAATCCCAAATTTACAGGTTCTGGGTTT
CCGAACCATATCTAAAAATCGGTAGAAGCCATACTCTATACACCCACATAACCCCAGATGCTGTTCCT
CAATTGCCTAAGGAATGTACTCTGAAACATTTGAGTTCTTACATGGAAGAGAAGTTAAAAAGTATGGA

ATCTAAAAAGAACATTGAAAGTGGTAAGTACGAATTTGACGTAGATTCCTCTGAGACCGATTCAACAA
AAGACGATGGAAAGCCTGACGATGATGATGATGATGACGACAACTTTGACGATGATGACAATTTTGAT
GATGACACGGTAGAGGAGGAAGACGCCAGTGGGGATCTGTTCAAGAATGAGAAGAAGGATGAAAATAA
AGAGTACCCTTATGACGTTCCAGACTACGCTTATCCTTACGACGTCCCCGACTACGCGTATCCCTACG
ACGTTCCTGATTACGCTTGAgcgatcgcggattataaagatgatgat. This gene block was inserted into the *AsiSI* site in the modified pJAZZ vector using Gibson assembly, resulting in the plasmid pEXP2^{apt}. The plasmid was co-transfected into NF54^{attB} parasites[33] with pUF-Cas9-EXP2-CT-gRNA. 1 μM aTc was maintained in the medium from the time of transfection and selection was applied with 2.5 μg/ml Blasticidin-S 24 h post transfection. After parasites returned from selection, proper integration was confirmed with the following primers (A, B, C and D respectively in Supplementary Fig. 1): GATCATCTCTTATATTAATAGGAATATATGATTTTTCACT, GCTCCGGCAAATGACAAGGG, CGGTCTCAGTGGTGTACGGTA, and TCACTTATGTTGTATAGAGACACAATTCGT. A clonal line was derived by limiting dilution and designated EXP2^{apt}.

For generation of the HSP101^{DDD} fusion in the NF54^{attB} parasite background, a gRNA target site was chosen just upstream of the *hsp101* stop codon (TAATAGTAAAGCTAAAAACT) and the gRNA seed sequence was synthesized as a sense and anti-sense primer pair (sense shown) TAAGTATATAATATTTAATAGTAAAGCTAAAAACTGTTTTAGAGCTAGAA, annealed and inserted into the *BtgZI* site of the plasmid pAIO, resulting in the plasmid pAIO-HSP101-CT-gRNA. To integrate the DHFR-based destabilization domain (DDD) at the 3' end of *hsp101*, a 5' homology flank (up to but not including the stop codon) was amplified from NF54^{attB} genomic DNA using primers GACGCGAGGAAAATTAGCATGCATCCTTAAGGAGATTCTGGTATGCCACTTGGTTC and CGTATGGGTACCTAGGGGTCTTAGATAAGTTTATAACTAAGTTTTTAGCTTTACTATT, incorporating a synonymous shield mutation in the protospacer adjustment motif of the gRNA target site within the *hsp101* coding sequence. A 3' homology flank (beginning 3 bp downstream of the stop codon) was amplified using primers CACTATAGAACTCGAGAATTACGCATATATATATATATATATATATAACATGGGTTG and GAACCAAGTGGCATACCAGAATCTCCTTAAGGATGCATGCTAATTTTCCTCGCGTC. The flank amplicons were assembled in a second PCR reaction using primers CACTATAGAACTCGAGAATTACGCATATATATATATATATATATATAACATGGGTTG and CGTATGGGTACCTAGGGGTCTTAGATAAGTTTATAACTAAGTTTTTAGCTTTACTATT and inserted between *XhoI* and *AvrII* in pPM2GT-3xHA-DDD[5], resulting in the plasmid pPM2GT-HSP101–3xHA-DDD. The 3xHA sequence was then replaced with a 3xFLAG sequence using a QuikChange Lightning Multi Site Directed Mutagenesis kit (Agilent) and the primer CTTAGTTATAAACTTATCTAAGACCCCTAGGGACTACAAGGACGACGACGACAAGGATTATAAAGATG ATGATGATAAAGATTATAAAGATGATGATGATAAAATCAGTCTGATTGCGGCGTTAG, resulting in the plasmid pPM2GT-HSP101–3xFLAG-DDD. This plasmid was linearized at the *AflII* site between the 3' and 5' homology flanks and co-transfected with pAIO-HSP101-CT-gRNA into NF54^{attB} and selection was applied with 10 μM trimethoprim 24 h post-transfection. A clonal line was isolated by limiting dilution after parasites returned from selection and designated NF54^{attB}::HSP101^{DDD}.

To generate an endogenous 3xFLAG tag at the HSP101 C-terminus of NF54^{attB} and EXP2^{apt} parasites, the DDD was removed from the plasmid pPM2GT-HSP101–3xFLAG-DDD using a QuikChange Lightning Multi Site Directed Mutagenesis kit and the primer GGATTATAAAGATGATGATGATAAAGATTATAAAGATGATGATGATAAATGACGGCCGCGTCGAGTTATATAATATATTTATG, resulting in the plasmid pPM2GT-HSP101–3xFLAG. This plasmid was linearized at the *AflII* site between flanks and co-transfected with pAIO-HSP101-CT-gRNA into NF54^{attB} and EXP2^{apt} parasites. Selection was applied with 10 nM WR99210 24 h post-transfection and clonal lines were isolated by limiting dilution after parasites returned from selection, resulting in the lines NF54^{attB}::HSP101–3xFLAG and EXP2^{apt}::HSP101–3xFLAG.

To facilitate integration of complementing second copies of EXP2 into the benign *cg6* locus of NF54^{attB} through integrase mediated attB x attP recombination[33], the attP sequence was first inserted into the plasmid pyEOE[34] using a QuikChange Lightning Multi Site Directed Mutagenesis kit and the primer GGTCGACTCTAGAGGATCCCCGGGTACCGAGCTCGAATTCTGGTTTGTCTGGTCAACCACCGCGGTCTCAGTGGTGTACGGTACAAACCCGAATTCTGGTTTGTCTGGTCAACCACCGCGGTCTCAGTGGTGTACGGTACAAACCCGGAATTCTAGATTTAATAAATATGTTCTTATATATAATG resulting in the plasmid pyEOE-attP. The full length *exp2* coding sequence without introns was amplified from NF54^{attB} cDNA with primers CGAATAAACACGATTTTTTCTCGAGATGAAAGTCAGTTATATATTTTCCTTTTTTTTGTTATTCTTCG and TAACTCGACGCGGCCGCTCACAGGTCCTCCTCGGAGATCAGCTTCTGCTCCTCGGCCCTAGCACCGTTCAAGTCTTCCTCGGAGATTAGCTTTTGTTCACCGTTCAAATCTTCTTCAGAAATCAACTTTTGTTCGCTAGCTTCTTTATTTTCATCTTTTTTTTCATTTTTAAATAAATCTCCACTG to introduce a 3xMYC tag and inserted into pyEOE-attP between *XhoI* and *EagI*, resulting in the plasmid pyEOE-attP-EXP2–3xMYC. A truncated version of the *exp2* coding sequence ending at codon position 233 was subsequently amplified with primers CGAATAAACACGATTTTTTCTCGAGATGAAAGTCAGTTATATATTTTCCTTTTTTTTGTTATTCTTCG and AATCAACTTTTGTTCGCTAGCATCTACATCAAACTCATATTTTCCACTTTC and inserted into this vector between *XhoI* and *NheI*, resulting in the plasmid pyEOE-attP-EXP2Δ234–287-3xMYC. These plasmids and the pyEOE-attP empty vector were each co-transfected with pINT[35] into EXP2^{apt}::HSP101–3xFLAG parasites or NF54^{attB} at the mature schizont stage using program U-033 on a Nucleofector 2b and Basic Parasite Nucleofector kit 2 (Lonza). Selection with 2μM DSM1[32] was applied 24 h post transfection (in addition to 2.5 μg/ml Blasticidin-S and 1 μM aTc for maintenance of endogenous EXP2 control by the aptamer system). Following return from selection, parasites were cloned by limiting dilution and expression of EXP2 second copies was confirmed by western blot.

For split GFP assays, the GFP1–10 sequence containing the SERA5 signal peptide for secretion into the PV was synthesized as a gene block (signal peptide in lowercase): atgaagagttatatttcgctcttctttatcttgtgcgtcatcttcaataagaatgtcatcaaatgtactggcgagagtATGAGCAAAGGAGAAGAACTTTTCACTGGAGTTGTCCCAATTCTTGTTGAATTAGATGGTGATGTTAATGGGCACAAATTTTCTGTCAGAGGAGAGGGTGAAGGTGATGCTACAATCGGAAAACTCACCCTTAAATTTATTTGCACTACTGGAAAACTACCTGTTCCATGGCCAACACTTGTCACTACTCTGAC

CTATGGTGTTCAATGCTTTTCCCGTTATCCGGATCACATGAAAAGGCATGACTTTTTCAAGAGTGCCA
TGCCCGAAGGTTATGTACAGGAACGCACTATATCTTTCAAAGATGACGGGAAATACAAGACGCGTGCT
GTAGTCAAGTTTGAAGGTGATACCCTTGTTAATCGTATCGAGTTAAAGGGTACTGATTTTAAAGAAGA
TGGAAACATTCTCGGACACAAACTCGAGTACAACTTTAACTCACACAATGTATACATCACGGCAGACA
AACAAAAGAATGGAATCAAAGCTAACTTCACAGTTCGCCACAACGTTGAAGATGGTTCCGTTCAACTA
GCAGACCATTATCAACAAAATACTCCAATTGGCGATGGCCCTGTCCTTTTACCAGACAACCATTACCT
GTCGACACAAACTGTCCTTTCGAAAGATCCCAACGAAAAGTAA. The *gfp1–10* sequence was PCR amplified with or without the *sera5* signal peptide using forward primers AAATATATCACCTAGGATGAAGAGTTATATTTCGCTCTTCTTTATCTTGTGC or AAATATATCACCTAGGATGAGCAAAGGAGAAGAACTTTTC, respectively, and the reverse primer ATAACTCGACCTTAAGTTACTTTTCGTTGGGATCTTTCGAAAGGACAG and each amplicon was inserted between *AvrII* and *AflII* in the plasmid pLN-ENR-GFP[35]. The resulting plasmids pLN-spGFP1–10 and pLN-cytGFP1–10, respectively (which also contain the attP sequence), were co-transfected with pINT into NF54^{attB} parasites and selection with 2.5 μg/ml Blasticidin-S was applied 24 h post transfection. A clone was derived by limiting dilution from each resulting parasite population and designated spGFP1–10 or cytGFP1–10, respectively. For tagging endogenous PTEX components with GFP11, the 3xHA-GFP11 sequence was synthesized as the gene block
CCTAGGTACCCGTACGACGTCCCGGACTACGCTGGCTATCCCTATGATGTGCCCGATTATGCGTATCC
TTACGATGTTCCAGATTATGCCGATGGAGGGTCTGGTGGCGGATCAACAAGTCGTGACCACATGGTCC
TTCATGAGTACGTAAATGCTGCTGGGATTACATAACGGCCG, PCR amplified with primers GATGAAAATAAAGAACCTAGGTACCCGTACGACGTCCCG and TAACTCGACGCGGCCGTTATGTAATCCCAGCAGCATTTACG and inserted between *AvrII* and *EagI* in pyPM2GT-EXP2-mNeonGreen[24], replacing *mNeonGreen* and resulting in the plasmid pyPM2GT-EXP2–3xHA-GFP11. Flanks targeting the 3’ end of *hsp101* were PCR amplified from pPM2GT-HSP101–3xFLAG using primers CACTATAGAACTCGAGAATTACGCATATATATATATATATATATATAACATGGGTTG and GACGTCGTACGGGTACCTAGGGGTCTTAGATAAGTTTATAACTAAGTTTTTAGC and inserted between *XhoI* and *AvrII* in pyPM2GT-EXP2–3xHA-GFP11, resulting in the plasmid pyPM2GT-HSP101–3xHA-GFP11. To edit the 3’ end of *ptex150*, a gRNA target site was chosen just downstream of the *ptex150* stop codon (TGGGAACCTCTTGTGTTTTA) and the gRNA seed sequence was synthesized as a sense and anti-sense primer pair (sense shown) TAAGTATATAATATTTGGGAACCTCTTGTGTTTTAGTTTTAGAGCTAGAA, annealed and inserted into the *BtgZI* site of pAIO, resulting in the plasmid pAIO-PTEX150-CT-gRNA. A 5’ homology flank (up to but not including the stop codon) was amplified from NF54^{attB} genomic DNA using primers GCCTTATAATCGTTCCTTTTGAGAACCTTAAGCTTCTTAGGACAAAATGGTACATATC and GACGTCGTACGGGTACCTAGGGTTATCATCTTCTTCTTCGTCTAATTCTTCTTCATC. A 3’ homology flank beginning just downstream of the gRNA target site was amplified using primers CACTATAGAACTCGAGGGTATAGAAAAAATATATAATATTTATATGCTTTTCTGCC and GATATGTACCATTTTGTCCTAAGAAGCTTAAGGTTCTCAAAAGGAACGATTATAAGGC. The flank amplicons were assembled in a second PCR reaction using primers CACTATAGAACTCGAGGGTATAGAAAAAATATATAATATTTATATGCTTTTCTGCC and GACGTCGTACGGGTACCTAGGGTTATCATCTTCTTCTTCGTCTAATTCTTCTTCATC and inserted

between *XhoI* and *AvrII* in pyPM2GT-EXP2–3xHA-GFP11, resulting in the plasmid pyPM2GT-PTEX150–3xHA-GFP11. These GFP11 tagging plasmids were each linearized at the *AflII* site introduced between the 3' and 5' homology flanks and co-transfected with their respective EXP2, HSP101 or PTEX150 Cas9/gRNA plasmids into spGFP1–10 and cytGFP1–10 parasites. Selection was applied with 2μM DSM1 24 h post-transfection and clonal lines were isolated by limiting dilution after parasites returned from selection.

Antibodies

The following antibodies were used for IFA and western blot at the indicated dilutions: rabbit polyclonal anti-HA SG77 (ThermoFisher) (WB: 1:1000); mouse anti-FLAG mAb clone M2 (Sigma) (IFA: 1:500, WB 1:500); rabbit mAb anti-FLAG 8H8L17 (ThermoFisher) (WB: 1:500); mouse anti-EXP2 mAb clone 7.7[36] (WB: 1:1000); mouse anti-HRP2 mAb 2G12[37] (IFA 1:500); rabbit polyclonal anti-SBP1[38] (IFA: 1:500); rabbit polyclonal anti-PfHAD1[39] (WB: 1:500); mouse anti-cMYC mAb 9E10 (ThermoFisher) (WB: 1:300); rabbit polyclonal anti-*Plasmodium* Aldolase ab38905 (Abcam) (IFA: 1:1000).

Parasite growth assays

Following extensive aTc washout, parasites were plated with or without 1μM aTc in triplicate at an initial parasitemia of 1%. Media was changed every 48 h and 1:1 subculture was performed as needed (generally every other day beginning at 96 h) to avoid culture overgrowth. Parasitemia (percent of total RBCs infected) was measured every 24 h by flow cytometry on a FACSCanto (BD Biosciences) by nucleic acid staining of cultured RBCs with phosphate buffered saline (PBS) containing 0.8 μg/ml acridine orange (gating strategy is shown in Supplemental Fig. 13). Cumulative parasitemias were back calculated based on the subculture schedule and data were fit to an exponential growth equation to determine rate constants using Prism (Graphpad).

IFA and quantification of protein export

For evaluation of protein export by IFA, mature schizonts were purified on an LD column using a QuadroMACs magnetic separator (Miltenyi Biotech) and allowed to invade fresh, uninfected RBCs with shaking for 3 hours before treatment with 5% w/v D-sorbitol to destroy unruptured schizonts. Pulse-invaded cells were washed extensively to remove aTc and then plated with or without 1 μM aTc and allowed to develop 24 h post invasion. Cells were fixed with PBS containing 4% paraformaldehyde and 0.0075% glutaraldehyde (for detection of HRP2) or cold 100% acetone (for detection of SBP1) and processed for IFA as described[5]. Primary antibody solutions contained either mouse anti-HRP2 and rabbit anti-*Plasmodium* aldolase (to mark the parasite and PV, see below) or rabbit anti-SBP1 and mouse anti-FLAG (detecting HSP101–3xFLAG to mark the PVM). After washing, secondary antibody incubation was carried out for one hour with Alexa Fluor anti-mouse 594 and anti-rabbit 488 IgG antibodies (for HRP2 experiments) or anti-rabbit 594 and anti-mouse 488 IgG antibodies (for SBP1 experiments) (Life Technologies), each diluted 1:2000. After final washing, coverslips were mounted using Pro-long antifade Gold with DAPI (Life Technologies). Images were collected with an ORCA-ER CCD camera (Hamamatsu) using AxioVision software on an Axio Imager.M1 microscope (Zeiss) with a 100x oil immersion objective using the same exposure times for each image (100 ms for HRP2–594 and 150 ms

for Aldolase-488 for HRP2 experiments or 300 ms for SBP1–594 and 150 ms for FLAG-488 for SBP1 experiments). Ten images were acquired for each condition using the DAPI channel for field selection to avoid bias. Images were then analyzed using Volocity 6.3 (PerkinElmer).

The border of each single-infected erythrocyte was traced using the DIC channel as a guide to define a region of interest (ROI). In HRP2 export experiments, the parasite was marked using the "find objects" measurement tool for the strong cytosolic signal from the *Plasmodium* aldolase-488 channel (automatic threshold setting with threshold offset set to −40% and minimum object size set to 0.5 μm^2). Given the intimate apposition of the PVM to the PPM, the aldolase signal was found to be suitable for marking both compartments. The signal corresponding to exported HRP2 was determined for each infected erythrocyte by removing the HRP2 signal within the aldolase object boundary in each ROI using the "subtract" tool and the mean fluorescence intensity of the HRP2 signal remaining in each ROI was collected. In SBP1 experiments, the PVM was marked using the "find objects" measurement tool for the HSP101–3xFLAG-488 channel (automatic threshold setting with threshold offset set to −30% and minimum object size set to 0.5 μm^2). Individual Maurer's clefts were identified using the "find spots" measurement tool for the SBP1–594 channel (offset minimum spot intensity set to 40% and brightest spot within radius set to 0.5 μm). All spots within the PVM object boundary were then removed using the "subtract" measurement tool and the number and fluorescent intensity of the remaining spots in each ROI were collected. Six independent experiments were performed. Two representative experiments were quantified and the data were pooled and plotted with Prism.

Transmission electron microscopy

For ultrastructural analyses, infected RBCs were fixed in 2% paraformaldehyde/2.5% glutaraldehyde (Polysciences) in 100 mM sodium cacodylate buffer, pH 7.2 for 1 h at room temperature. Samples were washed in sodium cacodylate buffer at room temperature and postfixed in 1% osmium tetroxide (Polysciences) for 1 h. Samples were then rinsed extensively in dH_20 prior to *en bloc* staining with 1% aqueous uranyl acetate (Ted Pella) for 1 h. Following several rinses in dH_20, samples were dehydrated in a graded series of ethanol and embedded in Eponate 12 resin (Ted Pella). Sections of 95 nm were cut with a Leica Ultracut UCT ultramicrotome (Leica Microsystems), stained with uranyl acetate and lead citrate, and viewed on a JEOL 1200 EX transmission electron microscope (JEOL USA) equipped with an AMT 8-megapixel digital camera and AMT Image Capture Engine V602 software (Advanced Microscopy Techniques).

Time-resolved western blot and immunoprecipitation

For time-resolved analysis of EXP2 and HSP101 by western blot, magnet purified terminal schizonts were allowed to pulse-invade fresh RBCs with shaking for 4 hours before treatment with 5% w/v D-sorbitol to destroy unruptured schizonts. Synchronized cultures were harvested every 6 hours for the duration for the developmental cycle and the erythrocyte cytosol was released by treatment with cold PBS containing 0.025% saponin (Sigma). Pellets were stored at −80°C until all samples were collected and then processed in parallel for western blot. Pellets were lysed in RIPA buffer containing EDTA-free protease

inhibitor cocktail (Roche), briefly bath sonicated and then centrifuged to pellet hemozoin. Supernatants were lysed in sample buffer containing DTT and boiled before separation by SDS-PAGE. For immunoprecipitation, time-resolved samples were similarly prepared and pellets were lysed in PBS containing 0.4% Triton X-100 and EDTA-free protease inhibitory cocktail. Hemozoin was cleared and lysates were rotated overnight at 4°C with anti-FLAG M2 agarose (Sigma) equilibrated in the lysis buffer. After extensive washing, agarose beads were eluted by boiling in sample buffer without DTT (to minimized release of anti-FLAG IgG heavy and light chains) before separation by SDS-PAGE. Western blot imaging was carried out with an Odyssey infrared imaging system (Li-COR Biosciences). Detection of primary antibodies was achieved with IRDye 680- or 800-conjugated secondary antibodies (Li-COR Biosciences) used at 1:10,000. Signal quantification was performed with Image Studio software (Li-COR Biosciences).

Electrophysiology

Late stage parasites were liberated in their PVM after percoll isolation[40]. Briefly, 0.5 ml of culture (5% hematocrit, <5% parasitemia) was layered on 65% percoll. After a brief spin down cells were collected from the interface. The cells were washed 3x in culture medium and incubated in 200 µl isotonic "high-potassium" buffer (140 mM KCl, 5 mM NaCl, 0.4 mM $CaCl_2$, 0.4 mM $MgCl_2$, 25 mM HEPES, 4.5 mg/ml glucose, 0.5% Albumax II) for 1 hour. To confirm liberation from the host RBC, that often stays attached to the parasite, 66 nM phalloidin-Alexa488 (Invitrogen) was used in the "high-potassium" buffer to label the attached RBC. 50 µl of this cell suspension were added to 3 ml of buffer A in the observation dish (fluorodish, WPI). The dish was mounted on the stage of a Zeiss Observer D200, equipped with a 100× 1.45NA oil objective, a filter-set for Alexa 488 (excitation 450–490 nm, emission 500–550 nm) and a Coolsnap EZ2 camera (Photometrics). Images were recorded using Micro Manager 1.4.21 and 1.4.22 [REF [41]]. Pipettes were pulled using a Sutter instrument (Novato, CA) pipette puller from Borosilicate glass capillaries (outer diameter: 1.5 mm, inner diameter: 0.86mm, in factory fire-polished, Sutter instrument). As bath buffer 150 mM NaCl, 5 mM KCl, 1.4 mM $CaCl_2$, 1 mM $MgCl_2$, 20 mM HEPES NaOH (pH 7.4), 4.5 mg/ml glucose (buffer A) and as pipette buffer 155 mM CsCl, 1.4 mM $CaCl_2$, 1 mM $MgCl_2$, 20 mM HEPES NaOH (pH 7.4) (buffer B) were used, similar to Desai *et al*[8]. Permeability of the PVM channel to nutrient-sized molecules was tested with 155 mM N-Methyl-D-glucamine, 155 mM L-Glutamic acid, 1.4 mM $CaCl_2$, 1 mM $MgCl_2$, 5 mM HEPES NaOH (pH 7.4) (buffer O). Concentration of small inorganic charge carriers is thus ~30x reduced in buffer O compared to buffer A and B. Conductivities of buffers were measured at 24°C with a CDM230 Conductivity Meter (Radiometer Analytica): buffer A 17.3 mS/cm, buffer B 20.7 mS/cm, buffer O 5.23 mS/cm.

Electrophysiology data was recorded in pClamp10 using an Axopatch 200B, filtered at 10kHz (8-pole Bessel) and digitized at 50kHz using a digidata 1332A or 1550B4 (all Molecular Devices). Command voltage denotes the voltage dialed on the amplifier. Applied voltage is the voltage reduced by the product of current and access resistance (15–20 MOhm), necessary to plot the conductance voltage response correctly. Voltage convention for the data presented is bath to ground and voltages applied to the pipette. Data was analyzed using ClampFit10 and custom matlab scripts. Error for data shown in Fig. 3h, i was

calculated in Excel (version 2016, Microsoft), P value in Fig. 3i was calculated in R (version 3.5.0, R core Team) with the fisher.test function, otherwise Prism was used.

Unless otherwise noted, sub-conductance steps were identified as the peaks ('findpeaks' function of matlab) in a derivative (dt = 200 us) of the current trace filtered offline with a 500 Hz 8-pole Bessel filter. The difference of current before and after the step were recorded as step size.

The rapid voltage response of the PVM channel makes it difficult to reliably find the maximum current for the normalization of the current using a voltage step protocol. As an alternative, conductance normalized to the conductance at −20 mV was plotted here to reflect on the open probability of the channel. The mean current on the second half of the voltage step was subtracted by the mean current at 0 mV to adjust for drift and divided by the applied voltage. Normalization is done with the mean current of the second half of the step to −20 mV at the end of each sweep.

The conductance voltage curves were fit to a piecewise linear function in the form

$$G = \left(m_1 \cdot V + b_1\right) \cdot \left(V \le c_1\right) + \left(m_1 \cdot c_1 + b_1\right) \cdot \left(c_1 < V < c_2\right) + \left(\frac{m_1 \cdot c_1 + b_1 - b_2}{c_2} \cdot V + b_2\right) \cdot \left(c_2 \le V \le c_3\right) + \left(\frac{m_1 \cdot c_1 + b_1 - b_2}{c_2} \cdot c_3 + b_2\right) \cdot \left(c_3 < V\right)$$

where V is the voltage applied to the membrane and G is the conductance, m_1, m_2, b_1, b_2, c_1, c_2, c_3 are free fit parameters.

The plateau conductance around 0 mV (p_1) and at positive voltages (p_2) follow as:

$$p_1 = m_1 \cdot c_1 + b_1$$

$$p_2 = \frac{m_1 \cdot c_1 + b_1 - b_2}{c_2} \cdot c_3 + b_2$$

That allows the definition of a half-open conductance as:

$$G_{half} = \frac{p_1 + p_2}{2}$$

The half-open voltages ($V_{\text{half-open, positive}}$ and $V_{\text{half-open, negative}}$ for the two arms) follow from that:

$$V_{\text{half-open, negative}} = \frac{G_{half} - b_1}{m_1}$$

$$V_{\text{half-open, positive}} = \frac{\left(G_{half} - b_2\right) \cdot c_2}{m_1 \cdot c_1 + b_1 - b_2}$$

Apparent Gating charges (z_i) were calculated from the slopes m_1 and m_2 by comparing to the slope of the expression for the open probability p_o [REF [42]]:

$$p_o = 1/\left[1 + exp - \left(\frac{w + z_i e_0 V}{k_B T}\right)\right]$$

Where k_b is the Boltzmann constant, T the absolute temperature (298K), w the work needed to change conformation, and e_0 the elementary charge. Since the model assumes two states (open and closed) the conductance curves need to be rescaled such that the plateaus p_1 and p_2 represent open and closed. The slopes m_i thus become:

$$m_{i,\ scaled} = \frac{m_i}{p_1 - p_2}$$

The derivative of the expression at the half-open voltage gives:

$$z_i = \frac{4\ k_B T m_{i,scaled}}{e_0}$$

Data Availability Statement

The data that support the findings of this study are available from the corresponding authors upon request.

Code Availability Statement

Matlab R2015b (Mathworks) scripts as described in methods are available upon request.

Statistics and Reproducibility

Figure 1c-e and Supplementary Figure 9d: Exact P values < 0.001 were calculated using the T.DIST.2T function in Excel for Mac (version 15.38, Microsoft).

Figure 3a: Presence of PVM around released parasite was observed in 3 independent experiments. The observation was published previously with the same technique[24]. Approximately 100 parasites were inspected and found to be retained in their PVM. A representative example was imaged and chosen for the figure.

Figure 3b: The RBC membrane attached to the released parasite was generally visualized to verify the pipette was approaching the parasite. A representative image was chosen to demonstrate this approach.

Figure 3c: Organic ion permeability was observed in 4 of 8 independent patch clamp experiments. Of the 4 experiments with channel activity one showed single channel activity, shown in the figure, and was compared to an example of single channel activity seen with the salt solutions used in the rest of the work.

Figure 3d, e: Examples of channel activity were chosen to reflect the range of patch conductances found in the experiments (as shown in Supplementary Figure 6).

Figure 3f: The example was chosen from the recordings that were used to generate Figure 3g.

Figure 3h: f_{chan} is calculated from a series of independent patch clamp experiments, n = 25, 35, 35 and 31 for 10%, 40%, 100% and 150% EXP2 expression respectively.

Figure 3i: Bars denote f_{chan} calculated from independent patch clamp experiments, n=35 and 28 for $NF54^{attB}$ and $NF54^{attB}$::$HSP101^{DDD}$ –TMP, respectively. P value was calculated after Fisher[43] in R (version 3.5.0, R core Team) with the fisher.test function.

Supplementary Material

Refer to Web version on PubMed Central for supplementary material.

Acknowledgements

This work was supported in part by NIH grant HL133453 to J.R.B and in part by the Division of Intramural Research of the Eunice Kennedy Shriver National Institute of Child Health and Human Development, National Institutes of Health. We thank Svetlana Glushakova for the creation and performance of the technique of vacuolar liberation, the performance of the IMF experiment, and many helpful conversations throughout the course of this project. We thank J. McBride, D. Cavanagh and EMRR for EXP2 antibody, D. Taylor for HRP2 antibody, C. Braun-Breton for SBP1 antibody, W. Beatty for assistance with electron microscopy, P. Gurnev for the buffer conductivity measurement, Paul Blank for helpful suggestions for the statistical treatment of the patch clamp data and B. Vaupel for technical assistance.

References

1. Lingelbach K & Joiner KA The parasitophorous vacuole membrane surrounding Plasmodium and Toxoplasma: an unusual compartment in infected cells. J Cell Sci 111 **(** Pt 11**)**, 1467–1475 (1998). [PubMed: 9580555] **()**
2. Desai SA Ion and nutrient uptake by malaria parasite-infected erythrocytes. Cellular microbiology 14, 1003–1009, doi:10.1111/j.1462-5822.2012.01790.x (2012). [PubMed: 22432505]
3. Sherling ES & van Ooij C Host cell remodeling by pathogens: the exomembrane system in Plasmodium-infected erythrocytes. FEMS Microbiol Rev 40, 701–721, doi:10.1093/femsre/fuw016 (2016). [PubMed: 27587718]
4. de Koning-Ward TF et al. A newly discovered protein export machine in malaria parasites. Nature 459, 945–949, doi:10.1038/nature08104 (2009). [PubMed: 19536257]
5. Beck JR, Muralidharan V, Oksman A & Goldberg DE PTEX component HSP101 mediates export of diverse malaria effectors into host erythrocytes. Nature 511, 592–595, doi:10.1038/nature13574 (2014). [PubMed: 25043010]
6. Elsworth B et al. PTEX is an essential nexus for protein export in malaria parasites. Nature 511, 587–591, doi:10.1038/nature13555 (2014). [PubMed: 25043043]
7. Kalanon M et al. The Plasmodium translocon of exported proteins component EXP2 is critical for establishing a patent malaria infection in mice. Cellular microbiology 18, 399–412, doi:10.1111/cmi.12520 (2016). [PubMed: 26347246]

8. Desai SA, Krogstad DJ & McCleskey EW A nutrient-permeable channel on the intraerythrocytic malaria parasite. Nature 362, 643–646, doi:10.1038/362643a0 (1993). [PubMed: 7681937]
9. Desai SA & Rosenberg RL Pore size of the malaria parasite's nutrient channel. Proceedings of the National Academy of Sciences of the United States of America 94, 2045–2049 (1997). [PubMed: 9050902]
10. Johnson D et al. Characterization of membrane proteins exported from Plasmodium falciparum into the host erythrocyte. Parasitology 109 **(** Pt 1**)**, 1–9 (1994). [PubMed: 8058359]
11. Bullen HE et al. Biosynthesis, localization, and macromolecular arrangement of the Plasmodium falciparum translocon of exported proteins (PTEX). The Journal of biological chemistry 287, 7871–7884, doi:10.1074/jbc.M111.328591 (2012). [PubMed: 22253438]
12. Hakamada K, Watanabe H, Kawano R, Noguchi K & Yohda M Expression and characterization of the Plasmodium translocon of the exported proteins component EXP2. Biochemical and biophysical research communications 482, 700–705, doi:10.1016/j.bbrc.2016.11.097 (2017). [PubMed: 27865834]
13. Gold DA et al. The Toxoplasma Dense Granule Proteins GRA17 and GRA23 Mediate the Movement of Small Molecules between the Host and the Parasitophorous Vacuole. Cell host & microbe 17, 642–652, doi:10.1016/j.chom.2015.04.003 (2015). [PubMed: 25974303]
14. Mesen-Ramirez P et al. Stable Translocation Intermediates Jam Global Protein Export in Plasmodium falciparum Parasites and Link the PTEX Component EXP2 with Translocation Activity. PLoS pathogens 12, e1005618, doi:10.1371/journal.ppat.1005618 (2016). [PubMed: 27168322]
15. Ganesan SM, Falla A, Goldfless SJ, Nasamu AS & Niles JC Synthetic RNA-protein modules integrated with native translation mechanisms to control gene expression in malaria parasites. Nature communications 7, 10727, doi:10.1038/ncomms10727 (2016).
16. Nasamu AS et al. Plasmepsins IX and X are essential and druggable mediators of malaria parasite egress and invasion. Science 358, 518–522, doi:10.1126/science.aan1478 (2017). [PubMed: 29074774]
17. Glushakova S et al. Hemoglobinopathic erythrocytes affect the intraerythrocytic multiplication of Plasmodium falciparum in vitro. The Journal of infectious diseases 210, 1100–1109, doi:10.1093/infdis/jiu203 (2014). [PubMed: 24688070]
18. Goldberg DE & Cowman AF Moving in and renovating: exporting proteins from Plasmodium into host erythrocytes. *Nature reviews.* Microbiology 8, 617–621, doi:10.1038/nrmicro2420 (2010). [PubMed: 20706280]
19. Kulzer S, Petersen W, Baser A, Mandel K & Przyborski JM Use of self-assembling GFP to determine protein topology and compartmentalisation in the Plasmodium falciparum-infected erythrocyte. Molecular and biochemical parasitology 187, 87–90, doi:10.1016/j.molbiopara.2012.11.004 (2013). [PubMed: 23271009]
20. Otto TD et al. New insights into the blood-stage transcriptome of Plasmodium falciparum using RNA-Seq. Molecular microbiology 76, 12–24, doi:10.1111/j.1365-2958.2009.07026.x (2010). [PubMed: 20141604]
21. Boddey JA & Cowman AF Plasmodium nesting: remaking the erythrocyte from the inside out. Annual review of microbiology 67, 243–269, doi:10.1146/annurev-micro-092412-155730 (2013).
22. Schwab JC, Beckers CJ & Joiner KA The parasitophorous vacuole membrane surrounding intracellular Toxoplasma gondii functions as a molecular sieve. Proceedings of the National Academy of Sciences of the United States of America 91, 509–513 (1994). [PubMed: 8290555]
23. Charpian S & Przyborski JM Protein transport across the parasitophorous vacuole of Plasmodium falciparum: into the great wide open. Traffic 9, 157–165, doi:10.1111/j.1600-0854.2007.00648.x (2008). [PubMed: 17944805]
24. Glushakova S et al. Exploitation of a newly-identified entry pathway into the malaria parasite-infected erythrocyte to inhibit parasite egress. Scientific reports 7, 12250, doi:10.1038/s41598-017-12258-x (2017). [PubMed: 28947749]
25. Ito D, Schureck MA & Desai SA An essential dual-function complex mediates erythrocyte invasion and channel-mediated nutrient uptake in malaria parasites. eLife 6, doi:10.7554/eLife.23485 (2017).

26. Garten M et al. Whole-GUV patch-clamping. Proceedings of the National Academy of Sciences of the United States of America 114, 328–333, doi:10.1073/pnas.1609142114 (2017). [PubMed: 28003462]
27. Levadny V, Aguilella VM & Belaya M Access resistance of a single conducting membrane channel. Biochim Biophys Acta 1368, 338–342 (1998). [PubMed: 9459610]
28. Hyun C, Rollings R & Li J Probing Access Resistance of Solid-state Nanopores with a Scanning Probe Microscope Tip. Small 8, 385–392, doi:10.1002/smll.201101337 (2012). [PubMed: 22393313]
29. Ho C et al. CryoEM Reveals Translocation Mechanism in Malaria Parasite Effector Export. Nature.
30. Klemba M, Beatty W, Gluzman I & Goldberg DE Trafficking of plasmepsin II to the food vacuole of the malaria parasite Plasmodium falciparum. The Journal of cell biology 164, 47–56, doi: 10.1083/jcb200307147 (2004). [PubMed: 14709539]
31. Spillman NJ, Beck JR, Ganesan SM, Niles JC & Goldberg DE The chaperonin TRiC forms an oligomeric complex in the malaria parasite cytosol. Cellular microbiology 19, doi:10.1111/cmi. 12719 (2017).
32. Ganesan SM et al. Yeast dihydroorotate dehydrogenase as a new selectable marker for Plasmodium falciparum transfection. Molecular and biochemical parasitology 177, 29–34, doi:10.1016/ j.molbiopara.2011.01.004 (2011). [PubMed: 21251930]
33. Adjalley SH et al. Quantitative assessment of Plasmodium falciparum sexual development reveals potent transmission-blocking activity by methylene blue. Proceedings of the National Academy of Sciences of the United States of America 108, E1214–1223, doi:10.1073/pnas.1112037108 (2011). [PubMed: 22042867]
34. Muralidharan V, Oksman A, Pal P, Lindquist S & Goldberg DE Plasmodium falciparum heat shock protein 110 stabilizes the asparagine repeat-rich parasite proteome during malarial fevers. Nature communications 3, 1310, doi:10.1038/ncomms2306 (2012).
35. Nkrumah LJ et al. Efficient site-specific integration in Plasmodium falciparum chromosomes mediated by mycobacteriophage Bxb1 integrase. Nature methods 3, 615–621, doi:10.1038/ nmeth904 (2006). [PubMed: 16862136]
36. Hall R et al. Antigens of the erythrocytes stages of the human malaria parasite Plasmodium falciparum detected by monoclonal antibodies. Molecular and biochemical parasitology 7, 247–265 (1983). [PubMed: 6350871]
37. Rock EP et al. Comparative analysis of the Plasmodium falciparum histidine-rich proteins HRP-I, HRP-II and HRP-III in malaria parasites of diverse origin. Parasitology 95 **(** Pt 2**)**, 209–227 (1987). [PubMed: 3320887]
38. Blisnick T et al. Pfsbp1, a Maurer's cleft Plasmodium falciparum protein, is associated with the erythrocyte skeleton. Molecular and biochemical parasitology 111, 107–121 (2000). [PubMed: 11087921]
39. Guggisberg AM et al. A sugar phosphatase regulates the methylerythritol phosphate (MEP) pathway in malaria parasites. Nature communications 5, 4467, doi:10.1038/ncomms5467 (2014).
40. Glushakova S, Yin D, Li T & Zimmerberg J Membrane transformation during malaria parasite release from human red blood cells. Curr Biol 15, 1645–1650, doi:10.1016/j.cub.2005.07.067 (2005). [PubMed: 16169486]
41. Edelstein AD et al. Advanced methods of microscope control using muManager software. J Biol Methods 1, doi:10.14440/jbm.2014.36 (2014).
42. Hodgkin AL & Huxley AF A quantitative description of membrane current and its application to conduction and excitation in nerve. J Physiol 117, 500–544 (1952). [PubMed: 12991237]
43. Fisher RA On the Interpretation of $\chi 2$ from Contingency Tables, and the Calculation of P. Journal of the Royal Statistical Society 85, 87–94, doi:10.2307/2340521 (1922).
44. Wilson EB Probable Inference, the Law of Succession, and Statistical Inference. Journal of the American Statistical Association 22, 209–212, doi:10.1080/01621459.1927.10502953 (1927).

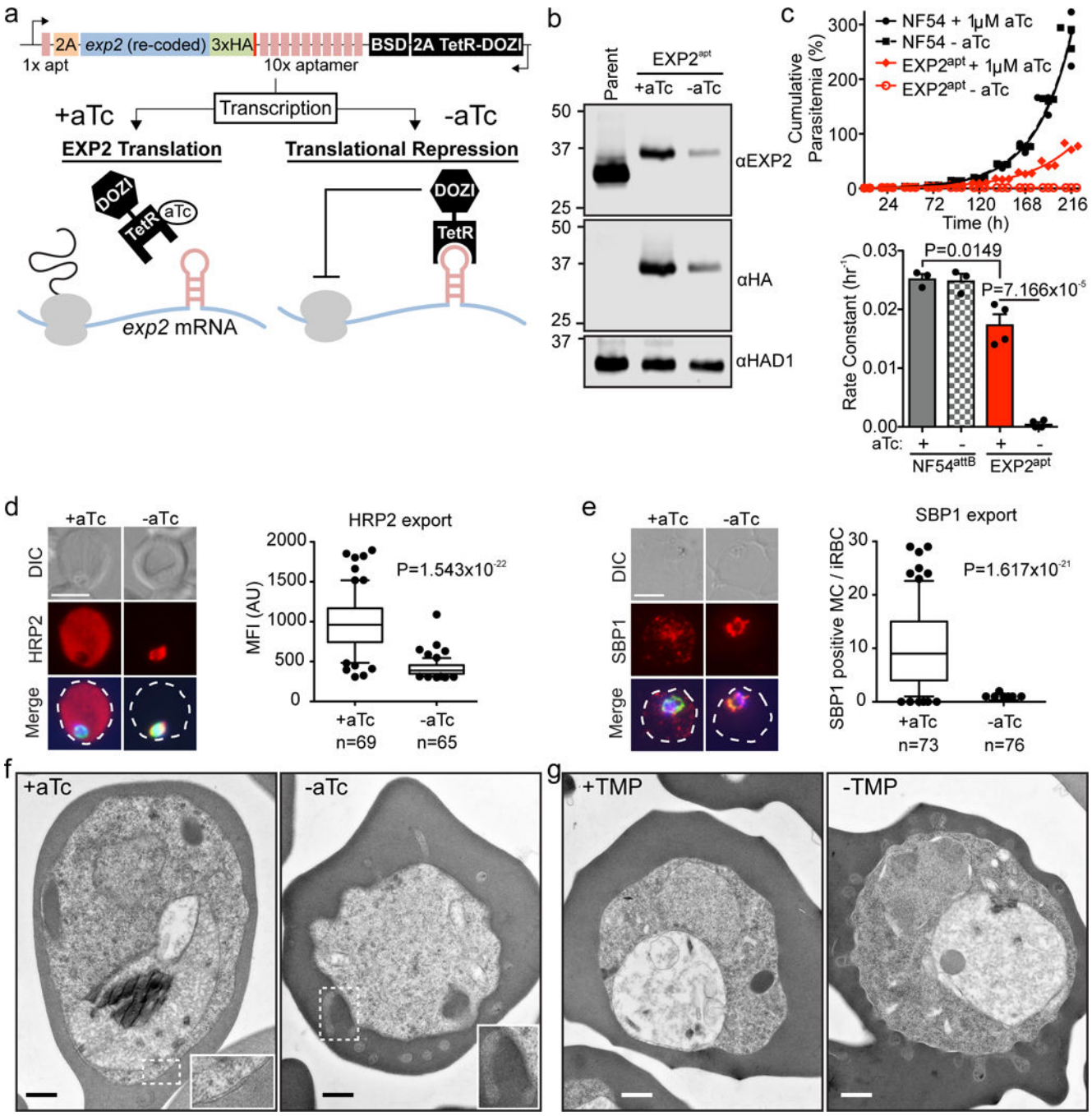

Figure 1. EXP2 is essential for blood stage survival and protein export.

a, Schematic of TetR-DOZI-aptamers strategy for conditional translational repression of EXP2. 2A, thosea asigna virus 2A skip peptide; HA, haemagglutinin tag; BSD, blasticidin-S deaminase; TetR-DOZI, Tetracycline repressor-DOZI fusion. **b,** Western blot of parental $NF54^{attB}$ - aTc and $EXP2^{apt}$ parasites +/− aTc for 48 h. The cytosolic haloacid dehalogenase-like hydrolase protein HAD1 serves as a loading control. Predicted molecular weights after signal peptide cleavage: EXP2: 30.8 kDa; EXP2–3xHA: 34.1 kDa. Results are representative of three independent experiments. EXP2 levels are reduced to 42.74±9.49%

+aTc and 6.49±3.95% -aTc relative to the parental line. Uncropped western blots are shown in Supplementary Fig. 11. **c,** Growth analysis of NF54^{attB} and EXP2^{apt} parasites +/− aTc. Results from one experiment with three technical replicates are shown and are representative of multiple independent experiments. Bar graph shows mean exponential growth rate constants (hr^{-1}) derived from the fit of three (NF54^{attB}) or four (EXP2^{apt}) independent experiments. Error bars indicate s.e.m. **d, e,** Immunofluorescence assay (IFA) showing export of the *Plasmodium* Export Element (PEXEL)-containing protein HRP2 (**d**) and the PEXEL-negative exported protein (PNEP) SBP1 (**e**) in EXP2^{apt} parasites (bearing a 3xFLAG tag on HSP101) synchronized to a 3 h invasion window and allowed to develop 24 h post invasion +/− aTc. Merge images include (d) Aldolase or (e) HSP101–3xFLAG in green and DAPI in blue. Scale bars, 5 μm. Quantification of HRP2 export to the host cytosol (**d**) or the number of SBP1-positive Maurer's Clefts (MC) (**e**) is shown. Data are pooled from two independent experiments, *n* is the number of individual parasite-infected RBCs. Boxes and whiskers delineate 25th-75th and 10th-90th percentiles, respectively. All *P* values determined by an unpaired, two-sided t-test. DIC, differential interference contrast; MFI, mean fluorescence intensity. **f, g,** PV morphological abnormalities following EXP2 knockdown (**f**) or HSP101 inactivation (**g**) visualized by transmission electron microscopy. The phenotype was visualized in three independent experiments by Giemsa stain (Supplementary Fig. 3) and in a single electron microscopy experiment. Scale bar, 500 nm.

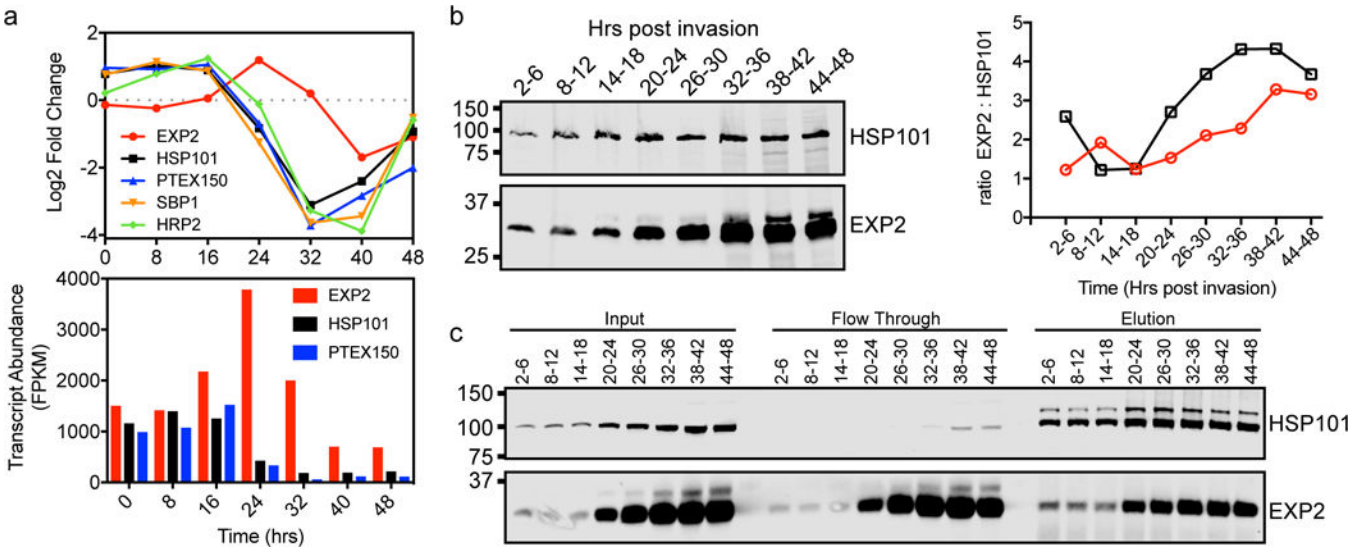

Figure 2. EXP2 expression differs from other PTEX components.

a, Transcript fold change of PTEX core components and exported proteins HRP2 and SBP1 throughout intraerythrocytic development gauged by RNA sequencing analysis of synchronized *P. falciparum* 3D7 parasites. Transcript abundance is shown for PTEX core components. Data from Otto *et al* dataset consisting of a single biological sample at each time point[20]. **b,** Time-resolved western blot detecting HSP101 and EXP2 in parasites with a 3xFLAG tag on the endogenous HSP101 C-terminus. Parasites were synchronized to a 4 h window by pulse-invasion. HSP101 and EXP2 were detected with anti-FLAG and anti-EXP2 antibodies, respectively. Data are representative of two independent experiments. Ratios of quantified EXP2 signal to HSP101 signal at each time point from two independent experiments (different symbols and colors) are given at right showing increasing levels of EXP2 relative to HSP101 in the second half of parasite development. **c,** Western blot of time-resolved immunoprecipitation of HSP101–3xFLAG and co-immunoprecipitation of EXP2. Parasites were synchronized as in **b**. Elution samples were not reduced to avoid release of anti-FLAG heavy and light chain from the beads and minor, higher molecular weight species of HSP101 are seen in these conditions. Data are representative of two independent experiments. Uncropped western blots are shown in Supplementary Fig. 11.

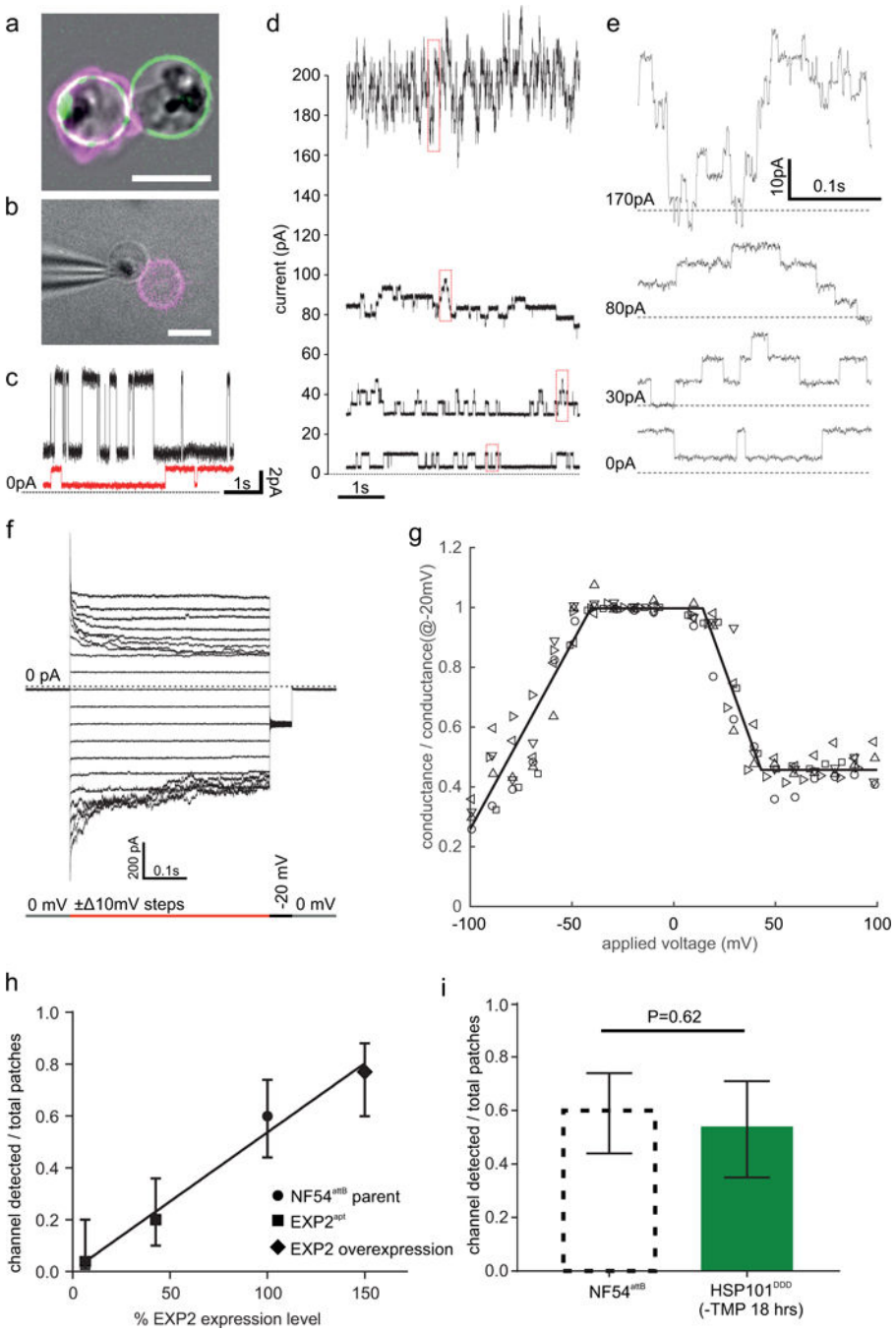

Figure 3. PVM channel characteristics and correlation with EXP2 levels.

a, Parasite liberation from the RBC within an intact PVM using a high potassium buffer shown with NF54^{attB}::EXP2-mNeonGreen parasites[24]. Green: EXP2-mNeonGreen marks the PVM. Magenta: Phalloidin-Alexa633 marks the RBC F-actin cytoskeleton. A double infected cell is shown where one parasite was released and the other remained within the host RBC. Zeiss 880 Airyscan image. **b,** The PVMs of released parasites (here NF54^{attB}) are patch clamped in an on-cell configuration. Magenta: Phalloidin-Alexa488 (epifluorescence). Gray: bright field. **c,** Single channel flickering with a command voltage of 30 mV applied to

the pipette using either small inorganic ions (black trace, buffer A and B in bath and pipette respectively) or amino acid and glucose-derived charge carriers (red trace, buffer O containing glutamic acid and N-methyl-D-glucamine in bath and pipette). Buffer O has a 3.6x lower conductivity and a ~30x reduced concentration of inorganic ions compared to the average of buffer A&B. The step size reduction shown here is 4.4x (6.54 pA to 1.47 pA) demonstrating that the PVM channel passes the nutrient ions of buffer O. **d,** Range of typical current fluctuations at 30 mV. **e,** Zoom in on the boxed (red) current recordings in **d**. **f,** Voltage response of a PVM channel ensemble. **g,** Conductance-voltage plot derived from the current-voltage response. Different symbols denote the 6 individual experiments used to create the plot. Solid line is a piecewise linear fit to all the data points. **h,** Correlation of the mean probability by which at least one channel is found in an experiment (f_{chan}) with the EXP2 abundance by western blot (solid line: linear regression R^2=0.98). The error bars denote the 95% CI calculated after Wilson[44]. **i,** f_{chan} in NF54^{attB}::HSP101^{DDD} 18h after TMP washout to inactivate HSP101 compared to NF54^{attB} parent line used in **h**. Error bars calculated after Wilson[44]. *P* value calculation detailed in Statistics and Reproducibility section. Scale bars in **a, b** are 5 μm. Current traces are filtered with a 500 Hz 8-pole Bessel filter for display. See the Statistics and Reproducibility section for information on the sample size.

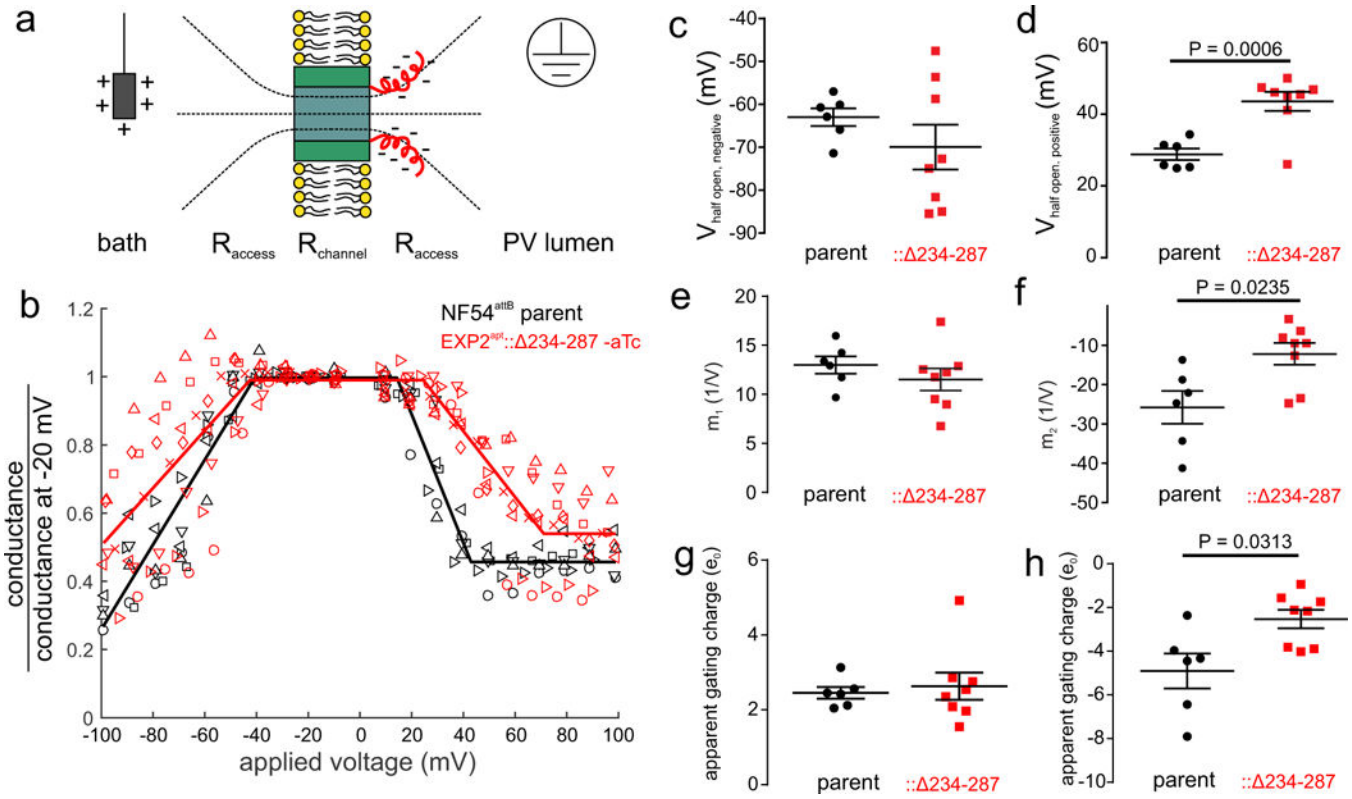

Figure 4. Altered voltage response of the PVM channel in EXP2^{apt}::Δ234–287 parasites.

a, Model for PVM channel gating by EXP2. Residues 234–287 (red), though not embedded in the bilayer (yellow) due to high charge, sense the electric field in the PV lumen due to the access resistance of the channel. This charge-sidedness can explain the asymmetry in the voltage response (Fig. 3g). Positive potential applied on the pipette electrode (gray box) would pull the C-terminus toward the bilayer while negative voltages would push the same residues away. As the electric field (dashed) drops non-linearly with distance from the channel mouth, it is to be expected that positive voltages pulling the C-terminus couple stronger than negative voltages pushing it away. Qualitatively this is consistent with the GV curve being asymmetric and responding stronger to positive voltages, as well as the increased variability in the statistics of the voltage response with the direction of the field. **b,** Conductance voltage plot of EXP2^{apt}::Δ234–287 (red, N=8 experiments) and the NF54^{attB} parent (black, N=6 experiments). Symbols distinguish experiments. Solid line is a piecewise linear fit to all combined experiments. **c, d,** Half-open voltage for negative voltages (**c**) and for positive voltages (**d**). **e, f,** Slopes at negative (**e**) and at positive (**f**) voltages. **g, h,** Apparent gating charges derived from the voltage response slope at negative voltages (**g**) and positive voltages (**h**). **c-h**, points are calculated from fits to individual traces of (**b**), P values are from an unpaired two-sided t-test, lines are mean±s.e.m.